

Bayesian Comparison of Interacting Scenarios

Antonella Cid^{a,b} Beethoven Santos^a Cassio Pigozzo^c Tassia Ferreira^d Jailson Alcaniz^{a,e}

^a *Observatório Nacional, 20921-400, Rio de Janeiro, RJ, Brasil.*

^b *Departamento de Física, Grupo Cosmología y Partículas Elementales, Universidad del Bío-Bío, Casilla 5-C, Concepción, Chile.*

^c *Instituto de Física, Universidade Federal da Bahia, 40210-340, Salvador, BA, Brasil.*

^d *PPGCosmo, CCE, Universidade Federal do Espírito Santo, 29075-910, Vitória, ES, Brasil.*

^e *Departamento de Física, Universidade Federal do Rio Grande do Norte, 59072-970, Natal, RN, Brasil*

E-mail: acidm@ubiobio.cl, thoven@on.br, cpigozzo@ufba.br,
t.ferreira@cosmo-ufes.org, alcaniz@on.br

Abstract. We perform a Bayesian model selection analysis for different classes of phenomenological coupled scenarios of dark matter and dark energy with linear and non-linear interacting terms. We use a combination of some of the latest cosmological data such as type Ia supernovae (SNe Ia), cosmic chronometers (CC), cosmic microwave background (CMB) and two sets of baryon acoustic oscillations measurements, namely, 2-dimensional angular measurements (BAO2) and 3-dimensional angle-averaged measurements (BAO3). We find weak and moderate evidence against two-thirds of the interacting scenarios considered with respect to Λ CDM when the full joint analysis is considered. About one-third of the models provide a description to the data as good as the one provided by the standard model. Our results also indicate that either SNe Ia, CC or BAO2 data by themselves are not able to distinguish among interacting models or Λ CDM but the standard BAO3 measurements and the combination with the CMB data are indeed able to discriminate among them. We find that evidence disfavoring interacting models is weaker when we use BAO2 (data claimed to be almost model-independent) instead of the standard BAO3 measurements. These results help select classes of viable and non-viable interacting models in light of current data.

Keywords: Interacting models, bayesian comparison, cosmological parameters

Contents

1	Introduction	1
2	Interacting Cosmological Scenarios	2
3	Data description	4
3.1	BAO data	4
3.2	CMB data	5
3.3	Cosmic chronometers	6
3.4	Supernovae Ia	7
3.5	Joint analysis	8
4	Methodology: Bayesian model selection	8
5	Analysis and Results	10
6	Final Remarks	16
A	BAO data	20

1 Introduction

In the coming decade cosmological data from a number of planned galaxy surveys and cosmic microwave background experiments will be used to tackle fundamental questions about the nature of the physical make-up of the Universe. Currently, the standard picture used to describe the available observations is the Λ CDM cosmology, a model in which most of the clustered matter is effectively collisionless (dark matter) with the bulk of the energy density of the Universe behaving like the vacuum energy, Λ (dark energy). With only half a dozen parameters, this remarkably simple model is able to explain most of the different sets of observations spanning over a large range of length scales (for a recent review, see [1]).

From the theoretical point of view, however, it is also well known that in order to provide a good description of the observed Universe the value of the vacuum energy density, $\rho_\Lambda \simeq 10^{-47} \text{ GeV}^4$, leads to an unsettled situation in the interface between Cosmology and Particle Physics, since it differs from theoretical expectations by 60-120 orders of magnitude [2]. Moreover, although the evolution of these two dark components over the cosmic time is significantly different, their current energy densities are of the same order, which gives rise to the question whether this is only a coincidence or has a more fundamental reason. Such questions are known as the cosmological constant problems [3]. Thus, given the theoretical uncertainties on the nature and behavior of the dark energy a number of mechanisms of cosmic acceleration have been investigated, including modifications of gravity on large scales or a possible interaction between the components of the dark sector.

In particular, interacting models of dark energy and dark matter [4–8] are based on the premise that no known symmetry in Nature prevents or suppresses a non-minimal coupling between these components and, therefore, such possibility must be investigated in light of

observational data¹ (for a recent review, see [9]). In some classes of these coupled models the coincidence problem above mentioned can be largely alleviated when compared with the standard cosmology. This was firstly discussed in reference [5], where the authors investigated asymptotic attractor behaviors for the ratio of the dark matter and dark energy densities. Since then, a number of interacting models with both numerical and analytical solutions have been proposed (see, e.g. [6–8, 10–12] and references therein).

In this paper, we study the observational viability of different classes of interacting scenarios, including both linear and non-linear interaction terms. In order to observationally distinguish between the different models we perform a Bayesian model selection analysis using current data of type Ia supernova (SN Ia) [13], measurements of the baryon acoustic oscillation (BAO) from the 6dFGS [14], SDSS-MGS [15], BOSS-LOWZ [16], BOSS-CMASS [16] and eBOSS [17] surveys, along with BAO measurements obtained from SDSS-DR7 [18], SDSS-DR10 [19], SDSS-DR11 [20], SDSS-DR12Q [21]; measurements of the expansion rate from cosmic chronometers [22] and the estimate of the sound horizon scale at the last scattering reported by the Planck collaboration [23]. We find weak and moderate evidence against some of the interacting scenarios studied with respect to Λ CDM when the full joint analysis is considered. We also discuss how such results can help select viable classes of interacting models.

The paper is organized as follows: in section 2 we present the classes of interacting models studied in this work. In section 3 we present the datasets considered in the analysis. The Bayesian approach used to evaluate the performance of the different interacting scenarios is described in section 4. Section 5 is devoted to the results of the Bayesian comparison analysis. Finally, our results are summarized in section 6.

2 Interacting Cosmological Scenarios

Let us consider a homogeneous, isotropic and flat cosmological scenario described by the Friedmann-Lemaître-Robertson-Walker metric (FLRW) and assume that the total energy-momentum tensor for the matter content of the universe is conserved. In the most general case, the total matter density is composed of radiation (r), baryons (b), dark matter (dm) and dark energy (x).

Also, let us suppose that the dark components are allowed to interact between each other through a phenomenological interaction term Γ :

$$\rho'_{dm} + \rho_{dm} = -\Gamma \quad \text{and} \quad \rho'_x + \gamma_x \rho_x = \Gamma, \quad (2.1)$$

where prime denotes a convenient derivative with respect to the function of the scale factor $\ln a^3$, γ_x is the barotropic index for dark energy and we adopt a pressureless dark matter component. Note that $\Gamma > 0$ indicate an energy transfer from dark matter to dark energy and $\Gamma < 0$ indicate the opposite. By adding equations (2.1) and taking $\rho = \rho_{dm} + \rho_x$ we find:

$$\rho' + \rho_{dm} + \gamma_x \rho_x = 0, \quad (2.2)$$

and, by rearranging the terms, we obtain:

$$\rho_{dm} = -\frac{\gamma_x \rho + \rho'}{1 - \gamma_x} \quad \text{and} \quad \rho_x = \frac{\rho + \rho'}{1 - \gamma_x}. \quad (2.3)$$

¹A usual critique to these scenarios is that, in the absence of a natural guidance from fundamental physics, one needs to specify a phenomenological interaction term between the dark components in order to establish a model and study their observational consequences.

Table 1. Definitions of the parameters b_1 , b_2 , b_3 for interactions $\Gamma(\rho, \rho', \rho'')$.

Interaction	b_1	b_2	b_3
$\Gamma_a = \alpha\rho_{dm} + \beta\rho_x$	$1 + \gamma_x + \alpha - \beta$	0	$\gamma_x + \alpha\gamma_x - \beta$
$\Gamma_b = \alpha\rho'_{dm} + \beta\rho'_x$	$(1 + \gamma_x + \alpha\gamma_x - \beta)/(1 + \alpha - \beta)$	0	$\gamma_x/(1 + \alpha - \beta)$
$\Gamma_c = \alpha\rho_{dm}\rho_x/\rho$	$1 + \gamma_x + \alpha(1 + \gamma_x)/(1 - \gamma_x)$	$\alpha/(1 - \gamma_x)$	$\gamma_x + \alpha\gamma_x/(1 - \gamma_x)$
$\Gamma_d = \alpha\rho_{dm}^2/\rho$	$1 + \gamma_x - 2\alpha\gamma_x/(1 - \gamma_x)$	$-\alpha/(1 - \gamma_x)$	$\gamma_x - \alpha\gamma_x^2/(1 - \gamma_x)$
$\Gamma_e = \alpha\rho_x^2/\rho$	$1 + \gamma_x - 2\alpha/(1 - \gamma_x)$	$-\alpha/(1 - \gamma_x)$	$\gamma_x - \alpha/(1 - \gamma_x)$

If we derivate any of equations (2.3) and replace (2.1) we can write a second order differential equation for a function $\Gamma = \Gamma(\rho, \rho', \rho'')$ [6]:

$$\rho'' + (1 + \gamma_x)\rho' + \gamma_x\rho = (1 - \gamma_x)\Gamma \quad \text{or} \quad \rho(\rho'' + b_1\rho' + b_3\rho) + b_2\rho^2 = 0, \quad (2.4)$$

where b_1 , b_2 , b_3 are constants, given in table 1, for the classes of interactions that are being considered in this work. The analytical solution of (2.4), describing the evolution of the dark sector [6], takes the following form:

$$\rho(a) = 3H_0^2(C_1a^{3\lambda_1} + C_2a^{3\lambda_2})^{1/(1+b_2)}, \quad (2.5)$$

where H_0 is the Hubble parameter and the constants C_1 , C_2 , λ_1 and λ_2 are given by:

$$C_1 = (\Omega_{dm0} + \Omega_{x0})^{1+b_2} - C_2, \quad C_2 = \frac{(\Omega_{dm0} + \gamma_x\Omega_{x0})(1 + b_2) + \lambda_1(\Omega_{dm0} + \Omega_{x0})}{(\Omega_{dm0} + \Omega_{x0})^{-b_2}(\lambda_1 - \lambda_2)}, \quad (2.6)$$

$$\lambda_1 = \frac{1}{2} \left(-b_1 - \sqrt{b_1^2 - 4b_3(1 + b_2)} \right), \quad \lambda_2 = \frac{1}{2} \left(-b_1 + \sqrt{b_1^2 - 4b_3(1 + b_2)} \right). \quad (2.7)$$

Throughout this paper, we use the dimensionless density parameters $\Omega_{i0} = \rho_{i0}/3H_0^2$ with the subscript 0 denoting their current values. It is worth emphasizing that the evolution of the dark sector is independent of that of radiation and baryons. Finally, the Hubble expansion rate in terms of the cosmological redshift z can be written as:

$$H(z) = H_0 \left(\Omega_{r0}(1+z)^4 + \Omega_{b0}(1+z)^3 + \left[C_1(1+z)^{-3\lambda_1} + C_2(1+z)^{-3\lambda_2} \right]^{\frac{1}{1+b_2}} \right)^{1/2}, \quad (2.8)$$

with $\Omega_{r0} + \Omega_{b0} + \Omega_{dm0} + \Omega_{x0} = 1$. Note that the radiation term includes the contribution of photons, $\Omega_{\gamma0}$, and neutrinos, $\Omega_{\nu0}$.

In reference [8] it was shown that the interacting models in table 1 can be described in a unified dark sector approach as a variable modified Chaplygin gas [24]. The authors point out that these scenarios can also be understood in terms of a varying barotropic index for the dark energy component. Furthermore, most of the interacting models shown in table 1 have been proposed in the literature in order to get a scaling solution for the coincidence problem, that is, in the context of these models the universe could approach a stationary stage at which the ratio between dark energy and dark matter densities becomes a constant. In particular, an interacting term of the type $\Gamma \propto \rho_{dm} + \rho_x$ was first introduced in references [4, 5] from a study of a suitable coupling between a quintessence scalar field and a pressureless cold dark matter

field. A generalization of this interaction was considered in reference [25] in order to overcome the coincidence problem near the transition time in a system that crosses the phantom divide line. On the other hand, the interaction $\Gamma \propto \rho'_{dm} + \rho'_x$ was first presented in reference [6] as a convenient scenario for alleviating the coincidence problem, with an analytical solution for the dark sector. The interaction Γ_c was firstly introduced in terms of a non-canonical scaling of the ratio of the dark matter and dark energy densities as an attempt to solve this same problem in reference [26]. This kind of interaction seems to be appealing since it is able to describe the large-scale evolution without instabilities or unphysical features [27]. Finally, interactions of the type Γ_d and Γ_e were studied in reference [12] in the realm of non-linear interactions alleviating the coincidence problem.

3 Data description

We focus on background data such as type Ia supernovae through the Joint Light-curve Analysis (JLA) compilation [13]; baryon acoustic oscillation data from 6dFGS [14], SDSS-MGS [15], BOSS-LOWZ [16], BOSS-CMASS [16] and eBOSS [17]; the cosmic chronometers reported in reference [22] and the angular scale of the sound horizon at the last scattering [23]. Furthermore, we independently consider BAO measurements obtained by the angular separation between pairs of galaxies [18–21]. In what follows, we briefly present each one of these datasets.

3.1 BAO data

In table 10 of Appendix A, the current available measurements of the BAO signal are shown in terms of the dimensionless ratio $d_z(z) = D_V(z)/r_s(z_d)$, where D_V is a combination of the line-of-sight and transverse distance scales defined in reference [28],

$$D_V(z) = \left((1+z)^2 D_A(z)^2 \frac{cz}{H(z)} \right)^{1/3}, \quad (3.1)$$

c is the speed of light, $D_A(z) = \frac{c}{(1+z)} \int_0^z \frac{dz}{H(z)}$ is the angular diameter distance, z_d is the redshift at the drag epoch and $r_s(z)$ is the comoving size of the sound horizon defined by:

$$r_s(z) = \int_z^\infty \frac{c_s dz}{H(z)}, \quad (3.2)$$

with $c_s = \frac{c}{\sqrt{3(1+\mathcal{R})}}$ being the sound speed of the photon-baryon fluid and $\mathcal{R} = \frac{3\Omega_b}{4\Omega_\gamma(1+z)}$ [29].

A relevant issue pointed out in the literature is the lack of informed correlations needed to use all the BAO data combined. In reference [15] the authors argue that SDDS-MGS [15] can be employed in combination with 6dFGS [14] and BOSS-LOWZ [16] because the overlapping volumes of the galaxy samples are small enough and consequently the correlations can be considered as negligible. Planck’s 2015 collaboration [30] uses these BAO data in addition to BOSS-CMASS [16] (uncorrelated) to constrain cosmological parameters. Here, we consider the BAO measurements used by the Planck collaboration as well as the recently reported eBOSS measurements (uncorrelated) – see table 10.

As we discuss in Appendix A, BAO measurements obtained through d_z use a fiducial model in order to convert angles into distances. This fact motivates the use of a different set of BAO measurements (claimed to be almost model-independent), which considers only the

transversal BAO signal through a geometrical feature such as the angular separation between pairs of galaxies,

$$\theta_{\text{BAO}}(z) = \frac{r_s(z_d)}{(1+z)D_A(z)}. \quad (3.3)$$

As explained in reference [19], in order to estimate θ_{BAO} from θ_{FIT} (completely model-independent measurement of the BAO signal obtained from the 2-point angular correlation function) a shift factor is needed, given that the redshift shell-width, δz , is different from zero. In reference [19] the model-dependence of the shift factor is tested for several cosmologies and the overall conclusion is that the shift factor is almost model-independent, with the difference between θ_{BAO} and θ_{FIT} being $\lesssim 2\%$ for the considered $\delta z \leq 0.02$. In this work we use fourteen θ_{BAO} measurements given in table 2 [18–21], and calculate the comoving size of the sound horizon taking the redshift at the drag epoch given by $z_d = 1059.6$, in accordance with Planck’s 2015 results [30]. From here on, we refer to BAO measurements of $d_z(z)$ as BAO3 and to BAO measurements of $\theta_{\text{BAO}}(z)$ as BAO2.

Data from the Sloan Digital Sky Survey (SDSS) were employed in obtaining BAO2 measurements (see table 2) as well as some of the BAO3 data points, such as SDSS-MGS, BOSS-LOWZ, BOSS-CMASS, eBOSS. Furthermore, although WiggleZ is an independent survey, in reference [31] the authors pointed out that the volumes considered in the WiggleZ survey and the BOSS-CMASS partially overlap and, as such, they calculated the corresponding correlations. Due to this fact, in this work we assume a conservative approach and do not combine BAO3 and BAO2 measurements.

Table 2. BAO measurements from angular separation of pairs of galaxies.

z	$\theta_{\text{BAO}}(z)$ [°]	Reference	z	$\theta_{\text{BAO}}(z)$ [°]	Reference
0.235	9.06 ± 0.23	[18] SDSS-DR7	0.550	4.25 ± 0.25	[19] SDSS-DR10
0.365	6.33 ± 0.22	[18] SDSS-DR7	0.570	4.59 ± 0.36	[20] SDSS-DR11
0.450	4.77 ± 0.17	[19] SDSS-DR10	0.590	4.39 ± 0.33	[20] SDSS-DR11
0.470	5.02 ± 0.25	[19] SDSS-DR10	0.610	3.85 ± 0.31	[20] SDSS-DR11
0.490	4.99 ± 0.21	[19] SDSS-DR10	0.630	3.90 ± 0.43	[20] SDSS-DR11
0.510	4.81 ± 0.17	[19] SDSS-DR10	0.650	3.55 ± 0.16	[20] SDSS-DR11
0.530	4.29 ± 0.30	[19] SDSS-DR10	2.225	1.85 ± 0.33	[21] SDSS-DR12Q

3.2 CMB data

To perform the full cosmic microwave background analysis building for the entire range of multipoles would require the study of all interacting models at a perturbative level, and also require the adaptation of Boltzmann codes such as CAMB or CLASS to obtain their anisotropy power spectrum. A simpler way to do that is to use the CMB compressed likelihood.

The compressed likelihood derived from Planck 2015 chains is composed by the set of parameters $\{R, \ell_a, \Omega_b h^2, n_s\}$ [23]. The shift parameter R is, by construction, very dependent on the matter dominated epoch. This is not evident in Planck’s analysis since all models studied have approximately the same behavior in that period. However, when we are dealing with interacting models, the dynamics of the matter dominated epoch is affected, so that constraining R to the values of reference [23] would include a bias on the analyses, and thereby artificially push the results to resemble the model with no interaction [23, 32]. In order to avoid this, we do not consider the shift parameter in our analysis. Besides, we do

not use the spectral index since it does not appear explicitly in our analysis and we fix the physical baryon density to $\Omega_b h^2 = 0.0226$, as reported in [33].

Consequently, this means that the only contribution of CMB data we consider is the angular scale of the sound horizon at the last scattering:

$$\ell_a = \frac{\pi}{\theta_*} = \frac{\pi(1+z_*)D_A(z_*)}{r_s(z_*)}, \quad (3.4)$$

where the comoving size of the sound horizon is evaluated at $z_* = 1089.9$, according with Planck's 2015 results [30]. We compare the value obtained in our study to the one reported by the Planck collaboration in 2015, $\ell_a = 301.63 \pm 0.15$ [23].

3.3 Cosmic chronometers

All data from cosmic chronometers used here were obtained through the differential age method (see table 3). We were careful to use only these measurements, and not to include those obtained with BAO so as not to double count information in the joint analyses.

The procedure consists of taking the relative age of passively evolving galaxies, with respect to the redshift, as suggested by reference [34]. Most of the values are obtained from the BC03 catalogue [35], but values from older releases were also used [36]. With the ratio between the differential ages, dt and the respective difference in redshift, dz , obtaining $H(z)$ becomes a simple task:

$$H(z) = -\frac{1}{1+z} \frac{dz}{dt}. \quad (3.5)$$

In our analysis, the theoretical value of $H(z)$ is given by equation (2.8). Note that we only use data of redshift up to < 1.2 . This is motivated by a discussion in reference [37], where the authors argue that the expansion history data of the universe might not be necessarily smooth outside $0.1 < z < 1.2$. Likewise, the authors of reference [38] have also shown that outside this range, the model of synthesis of stellar population adopted to derive the galaxy ages becomes relevant.

Table 3. Estimated values of $H(z)$ obtained using the differential age method.

z	$H(z)$	Ref.	z	$H(z)$	Ref.	z	$H(z)$	Ref.
0.07	69 ± 19.6	[39]	0.28	88.8 ± 36.6	[39]	0.48	97 ± 62	[40]
0.09	69 ± 12	[36]	0.352	83 ± 14	[38]	0.593	104 ± 13	[38]
0.12	68.6 ± 26.2	[39]	0.3802	83 ± 13.5	[22]	0.68	92 ± 8	[38]
0.17	83 ± 8	[36]	0.4	95 ± 17	[36]	0.781	105 ± 12	[38]
0.179	75 ± 4	[38]	0.4004	77 ± 10.2	[22]	0.875	125 ± 17	[38]
0.199	75 ± 5	[38]	0.4247	87.1 ± 11.2	[22]	0.88	90 ± 40	[40]
0.20	72.9 ± 29.6	[39]	0.4497	92.8 ± 12.9	[22]	0.9	117 ± 23	[36]
0.27	77 ± 14	[36]	0.4783	80.9 ± 9	[22]	1.037	154 ± 20	[38]

Notice that the cosmic chronometer is the only method providing cosmology-independent, direct measurements of the expansion history of the universe [37].

3.4 Supernovae Ia

The best probe of the expansion history of the Universe on large-scales (up to $z \lesssim 2$) is provided nowadays by observations of type Ia supernovae. The main reason for this is that SNe Ia are examples of "standardisable candles", due to the fact that their absolute magnitudes can be approximated by using light-curve templates to extract their stretch and color parameters. We use the JLA sample which contains a set of 740 spectroscopically confirmed SNe Ia [13] composed by several low-redshift ($z < 0.1$) samples, the full three-year SDSS-II supernova survey sample [41] in the interval $0.05 < z < 0.4$, the three-years data of the SNLS survey [42, 43] up to redshift $z < 1$ and some high-redshift Hubble Space Telescope SNe [44] with redshift $0.216 < z < 1.755$.

The predicted apparent magnitude of a SN Ia can be obtained from its light curve parameters through the linear relation:

$$m(z, \Theta) = \mu(z, \Theta) + M_B - \alpha_{\text{JLA}} \times x_1 + \beta_{\text{JLA}} \times c, \quad (3.6)$$

where Θ represents the set of parameters of the model, x_1 is the time stretching of the light curve and c is the supernova color at its maximum brightness. In the expression above, $\mu(z, \Theta)$ is the theoretical distance modulus, given by:

$$\mu(z, \Theta) = 5 \log \frac{d_L(z, \Theta)}{10 \text{ pc}}, \quad (3.7)$$

where $d_L(z, \Theta)$ is the luminosity distance:

$$d_L(z) = (1+z) \int_0^z \frac{dz'}{E(z')}, \quad (3.8)$$

and $E(z) \equiv H(z)/H_0$.

In equation (3.6), the light-curve parameters x_1 and c have different values for each supernova and are derived directly from the light-curves. However, the nuisance parameters M_B , α_{JLA} and β_{JLA} are assumed to be constant for all the supernovae but differ for each cosmological model. Additionally, since the properties of the host galaxy can generate some effects on the intrinsic brightness of the SNe Ia, we follow reference [13] and model the relation between M_B and the host galaxy stellar mass, M_{host} , by assuming $M_B \rightarrow M_B + \Delta_M$ if $\log_{10} M_{\text{host}} > 10$. Thus, the nuisance parameters corresponding to the measurements are α_{JLA} , β_{JLA} , M_B and Δ_M .

The analyses involving the JLA dataset were carried out by comparing the predicted magnitude $m(z, \Theta)$ from equation (3.6) against the observed ones of the JLA sample (table F.3 of reference [13]), which are denoted by $m_B(z)$ and represent the observed peak magnitude in rest-frame B band. The Monte Carlo analyses for the JLA SNe Ia sample were performed by assuming a multivariate Gaussian likelihood of the form

$$\mathcal{L}_{\text{JLA}}(D | \Theta) = \exp \left[-\chi_{\text{JLA}}^2(D | \Theta) / 2 \right], \quad (3.9)$$

with

$$\chi_{\text{JLA}}^2(\Theta) = [\mathbf{m}_B - \mathbf{m}(\Theta)]^T C^{-1} [\mathbf{m}_B - \mathbf{m}(\Theta)], \quad (3.10)$$

where C corresponds to the covariance matrix of the m_B measurements, estimated accounting for various statistical and systematic uncertainties (we refer the reader to reference [13] for more information about these uncertainties).

3.5 Joint analysis

By using the same methodology as in the case of the JLA SNe compilation, we consider a multivariate Gaussian likelihood for BAO2, BAO3, CC and CMB data. The chi-square function for the measurement of a generic function f is defined as follows:

$$\chi_f^2(\Theta) = \sum_i \left(\frac{f(z_i) - f(z_i, \Theta)}{\sigma_{f_i}} \right)^2, \quad (3.11)$$

where $f(z_i)$ represents the measured value for f at redshift z_i , whereas $f(z_i, \Theta)$ is computed assuming a model with parameters Θ . The function f stands for the functions $\theta_{\text{BAO}}(z)$, $d_z(z)$, $H(z)$ and $\ell_a(z_*)$ for BAO2, BAO3, CC and CMB data, respectively. The sum in equation (3.11) runs over the data in table 2 for BAO2 and table 3 for CC. For BAO3 we consider 6dFGS, SDSS-MGS, BOSS-LOWZ, BOSS-CMASS and eBOSS as described in section 3.1 and shown in table 10. For CMB, we take just a single data at z_* . In the case of the joint analysis, the total likelihood is obtained as the product of individual likelihoods associated to each data as in equation (3.9) by using the chi-square definition in equation (3.11). For example, the full joint analysis considering BAO2 data is given by: $\mathcal{L}_{\text{joint}} = \mathcal{L}_{m(z)} \times \mathcal{L}_{\theta_{\text{BAO}}(z)} \times \mathcal{L}_{H(z)} \times \mathcal{L}_{\ell_a(z_*)}$.

4 Methodology: Bayesian model selection

The Bayesian inference method constitutes a robust statistical technique for parameter estimation and model selection, and over the last years has been widely used in the study of cosmological scenarios [45–49]. Bayesian inference is based on the Bayes’ theorem, which updates our knowledge of a given model (or hypothesis) in light of new available data (or information). Mathematically, the Bayes’ theorem gives us the posterior probability P for a set of parameters Θ , given the data \mathcal{D} , described by a model \mathcal{M} ,

$$P(\Theta|\mathcal{D}, \mathcal{M}) = \frac{\mathcal{L}(\mathcal{D}|\Theta, \mathcal{M}) \mathcal{P}(\Theta|\mathcal{M})}{\mathcal{E}(\mathcal{D}|\mathcal{M})}, \quad (4.1)$$

where \mathcal{L} , \mathcal{P} and \mathcal{E} stand for the likelihood, prior and evidence, respectively.

The evidence in equation (4.1) constitutes just a normalization constant in the Bayesian parameter estimation approach, however, it becomes a key ingredient in the Bayesian model comparison approach. In order to compare the performance of different models given a set of data, we use the Bayes’ factor defined in terms of the evidence of models \mathcal{M}_i and \mathcal{M}_j as:

$$B_{ij} = \mathcal{E}_i/\mathcal{E}_j, \quad (4.2)$$

where the evidence corresponds to the average value of the likelihood over the entire model parameter space allowed, before we observe the new data [50], that is:

$$\mathcal{E}(\mathcal{D}|\mathcal{M}) = \int \mathcal{L}(\mathcal{D}|\Theta, \mathcal{M}) \mathcal{P}(\Theta|\mathcal{M}) d\Theta. \quad (4.3)$$

If the models \mathcal{M}_i and \mathcal{M}_j have the same prior probability, then the Bayes factor gives the posterior odds of the two models.

Monte Carlo sampling techniques are widely applied nowadays to construct the posterior distribution in equation (4.1), since it is very difficult to compute the posterior numerically (see references [51, 52] for applications of some Monte Carlo algorithms in cosmology). In

this sense, we performed the analyses involving the data described in section 3 by applying the nested sampling (NS) Monte Carlo algorithm [53], which is well known for its efficiency in the evidence computation since it is designed to directly estimate the relation between the likelihood function and the prior mass, thus obtaining the evidence (and its uncertainty) immediately by summation, while also computing the samples from the posterior distribution as an optional by-product. To compute the evidence values and generate the posterior distributions we used the MULTINEST² [54–56] algorithm, requiring a global log-evidence tolerance of 0.01 as a convergence criterion and working with a set of 1000 live points to improve the accuracy in the estimate of the evidence. With this number of live points, the number of samples for all posterior distributions was of order $\mathcal{O}(10^4)$.

The Jeffreys’ scale [57] gives us an empirical measure for interpreting the strength of the evidence in comparing two competing models. In order to perform model comparison in this work we use a conservative version of the Jeffreys’ scale defined in reference [58] (see table 4). Usually for $|B_{ij}| < 1$ the evidence in favor/against model \mathcal{M}_i relative to model \mathcal{M}_j is interpreted as inconclusive. On the other hand, the thresholds shown in table 4 for weak, moderate and strong evidences in favor/against the tested model correspond to posterior odds of about 3:1, 12:1 and 150:1, respectively [58]. Here, we take Λ CDM as the reference model \mathcal{M}_j , as such, the subscripts in the Bayes’ factor (4.2) will be omitted hereafter. Note that from now on, $\ln B < -1$ means support in favor of the Λ CDM model.

Table 4. The Jeffreys’ scale, empirical measure for interpreting the evidence in comparing two models \mathcal{M}_i and \mathcal{M}_j as presented in reference [58]. The left column indicates the threshold for the logarithm of the Bayes factor and the right column the interpretation for the strength of the evidence above the corresponding threshold.

$ \ln B_{ij} $	Interpretation
< 1	inconclusive
1	weak
2.5	moderate
5	strong

The priors considered in this work are shown in table 5. We have chosen a uniform prior for the parameters appearing in all the studied models such as Ω_{dm} , h , α_{JLA} , β_{JLA} , M_B and Δ_M , and a Gaussian prior for the parameters defining only some of the models, i.e., γ_x and the interacting parameters α and β . For the parameter Ω_{dm} we choose a conservative uniform prior between 0 and 1, for the dimensionless Hubble parameter h we adopt a range 10 times wider than the 1σ value reported by Riess et al. in reference [59], we emphasize that Riess’ result is considered only through this prior and not used as an independent data in the analysis. For the JLA parameters, α_{JLA} , β_{JLA} , M_B and Δ_M , we use a range 20 times wider than the 1σ values reported by Betoule et al. in reference [13]. The prior for the parameter γ_x corresponds to the 1σ value informed by Planck [30] and the prior for the interacting parameters is the same for all the studied models, of order 10^{-3} with a negative mean (see reference [8]), in such a way that most of the models in table 1, Γ_a , $\Gamma_c - \Gamma_e$, favor a transfer from dark energy to dark matter provided that ρ_{dm} and ρ_x are positive defined. This kind of transfer is expected for some interacting models based on thermodynamical arguments [60].

²<https://ccpforge.cse.rl.ac.uk/gf/project/multinest>.

Given that we expect interacting models not to affect the physics of the primordial universe but only to modify the evolution of the dark sector recently, we fix the following parameters: $\Omega_b h^2 = 0.0226$ [33], $\Omega_\gamma h^2 = 2.469 \times 10^{-5}$ [61], $\Omega_r = \Omega_\gamma \left(1 + \frac{7}{8} \left(\frac{4}{11}\right)^{\frac{4}{3}} N_{\text{eff}}\right)$, $N_{\text{eff}} = 3.046$ [62]. Moreover, for the redshift at the drag epoch and last scattering we use the Planck values [30]: $z_d = 1059.60$ and $z_* = 1089.90$, respectively.

Table 5. Priors on the free parameters of the studied models. For a Gaussian prior we inform (μ, σ^2) and for a Uniform prior (a, b) represent $a \leq x \leq b$.

Parameter	Status	Prior	Ref.
Ω_{dm0}	Global Parameter	Uniform: (0, 1)	-
h	Global Parameter	Uniform: (0.5584, 0.9064)	[59]
γ_x	Variable state parameter	Gaussian: (-0.006, 0.002)	[30]
α	Interacting models	Gaussian: (-0.001, 0.01)	[8]
β	Interacting models	Gaussian: (-0.001, 0.01)	[8]
α_{JLA}	Global, JLA parameter	Uniform: (0.021, 0.261)	[13]
β_{JLA}	Global, JLA parameter	Uniform: (1.601, 4.601)	[13]
M_B	Global, JLA parameter	Uniform: (-19.45, -18.65)	[13]
ΔM	Global, JLA parameter	Uniform: (-0.53, 0.39)	[13]

5 Analysis and Results

We perform a Bayesian comparison analysis of the interacting models presented in table 1 in terms of the strength of the evidence according to Jeffreys' scale (see table 4). In this study we used the priors shown in table 5 and considered different combinations of background data such as, type Ia supernovae, cosmic chronometers, baryon acoustic oscillations and cosmic microwave background. Our main results are summarized in tables 6-9. We labeled different realizations of models in table 1 with numerical subscripts as follows: 0, 1, 2, 3, 4 meaning $\gamma_x = 0$, $\beta = 0$, $\alpha = 0$, $\alpha = \beta$, $\alpha \neq \beta$, respectively. We do not include the analysis for the interacting model Γ_{b02} because it reduces to the Λ CDM scenario.

In table 6 we observe that by considering JLA, BAO2 or CC by themselves or even the joint analysis with BAO2 + CC, we get inconclusive evidence for the interacting models and for the ω CDM model when compared to Λ CDM. We remark that the BAO2 and CC data that were used are model-independent or almost model-independent, respectively, and these alone or jointly are not able to rule out any of the models considered in this work compared to Λ CDM. We also observe that by analyzing BAO2 + CC + CMB we find weak or moderate evidence disfavoring some of the interacting models.

In table 7 we show the logarithm of the Bayesian evidence and the interpretation of the strength of the evidence for the analysis with BAO3, BAO3 + CC and BAO3 + CC + CMB. We note that some of the interacting models are disfavored with a weak evidence in the studies with BAO3 and BAO3 + CC, and these evidences become moderate (in most of the cases) when we add CMB data to the analysis. Moreover, we notice that the models presenting inconclusive evidence in this analysis are the same as in the study of BAO2 + CC + CMB, which seems to indicate that the addition of the CMB data to the analysis, even when it is a single data point, contributes significantly to the evidence disfavoring most of the interacting models.

In tables 8 and 9 the results for the full joint analysis, including SNe Ia from JLA compilation, are shown considering independently the measurements of BAO2 and BAO3, respectively. We present the best fit parameters for the studied models, along with the logarithm of the Bayesian evidence, the logarithm of the Bayes' factor and the interpretation for the strength of the evidence. It is interesting to note that, for the results in table 8 as well as the results in table 9, the evidence remains inconclusive for the models ω CDM, Γ_{a02} , Γ_{c0} , Γ_{e0} , Γ_{a2} , Γ_{b2} , Γ_c and Γ_e when compared to Λ CDM. These models are the same as those presenting inconclusive evidence in the analyses BAO2 + CC + CMB and BAO3 + CC + CMB. Observe that the inconclusive models correspond to $\Gamma \propto \rho_x$ or $\Gamma \propto \rho'_x$ and the energy transfer for these models turns out to be from dark energy to dark matter.

We also notice that the moderated evidence found in the analysis BAO2 + CC + CMB becomes weak when we consider the full analysis including JLA. On the other hand, the weak evidences obtained in the analysis with JLA + BAO2 + CC + CMB become all moderate when we take BAO3, instead of BAO2 in the full joint analysis. This result is expected since BAO3 data implicitly seem to favor the Λ CDM scenario. It is worth pointing out here that the value of the Hubble parameter turns out to be higher for all the studied scenarios when we consider BAO2 instead of BAO3 in the full joint analysis (see tables 8 and 9), this seems to indicate that the BAO data play an important role in the H_0 tension [63], we also observe that the values of the fitted barotropic index and the interacting parameters are approximately one order of magnitude lower in the full joint analysis including BAO3 compared to the analysis with BAO2, which reinforce the indication for a preference of Λ CDM in BAO3 data.

In reference [8] some of the models studied in this work were analyzed in a joint analysis considering Union2.1 + BAO3 + H(z) + CMB, and a comparison among the models was performed using the Akaike and Bayesian information criteria (AIC and BIC, respectively). At this point, it is worth mentioning that, differently from these methods, the Bayesian model comparison applied in this analysis selects the best-fit model by comparing the compromise between quality of the fit and predictability, and by evaluating if the extra degrees of freedom of a given model are indeed required by the data, preferring the model that describes the data well over a large fraction of their prior volume. The results of [8] in terms of BIC indicate that the interacting models have "strong evidence against" when compared to Λ CDM and this strength of evidence changes to "evidence against" (or moderate) when compared to Λ CDM but using binned JLA data instead of Union2.1. Besides, the BAO measurements used included WiggleZ data, but the full JLA dataset was not considered. The authors also compared the interacting models with the ω CDM model obtaining "not enough evidence against" or inconclusive evidence for the interacting models with three free parameters analyzed (Γ_{a01} , Γ_{a02} , Γ_{a03} , Γ_{b01} , Γ_{c0} , Γ_{d0} and Γ_{e0} in this work). In our study, the evidence interpretation remains the same in most of the models when we compare them to ω CDM instead of Λ CDM, the only exceptions are Γ_{b4} in table 8 and Γ_{a3} in table 9. Finally, the ordering of the evidence in terms of the number of free parameters for the interacting models reported in reference [8] with the BIC approach is not observed in our work using a full Bayesian comparison approach.

In reference [45] the model Γ_{a01} was analyzed in a model comparison approach with JLA data and a different set of BAO3 measurements. The authors found moderate evidence in favor of this model compared to Λ CDM. Instead, in this work we found moderate evidence disfavoring the Γ_{a01} model. The main differences between our datasets and the ones used in reference [45] are that (i) we are considering CMB data and high redshift values of BAO2 and BAO3 data that have become available only recently. Furthermore, the authors of reference [45] used WiggleZ data, which is not considered in the set of BAO3 data used in this

work. Finally, the authors use the Eisenstein's approximation for the redshift at the drag epoch whereas here we use the Planck's value.

Lastly, in Fig. 1 we summarize our results in terms of the interpretation of the Bayes' factor considering the Jeffreys' scale. We show the Bayes' factor for the full joint analysis of the several realizations of interacting models in table 1 compared to Λ CDM. We consider independently the full joint analysis using BAO2 and BAO3 data. We notice that by considering BAO3 instead of BAO2 data shift the Bayes factor towards a better support for the Λ CDM model. For completeness, in Fig. 2 we show an example of contour plots and PDFs in our analysis (models Γ_{a02} and Γ_{a2}). The figures show the differences in parameter estimation considering BAO2 or BAO3 in the full joint analysis. We notice a tension in the parameter estimation using BAO2 or BAO3 for the model Γ_{a02} , this tension is slightly released when we enlarge the parameter space by adding the barotropic index γ_x to the analysis (model Γ_{a2}). This behavior is analogous for all the studied scenarios, and therefore the other contour plots are not shown for brevity.

Table 6. Bayesian evidence ($\ln \mathcal{E}$) for the models studied in this work. The interpretation of the evidence is inconclusive when not indicated. Note that $\ln \mathcal{E}_i - \ln \mathcal{E}_{\Lambda\text{CDM}} < -1$ favors Λ CDM.

Dataset	BAO2	CC	JLA	BAO2+CC	BAO2+CC+CMB	
Model	$\ln \mathcal{E}$	$\ln \mathcal{E}$	$\ln \mathcal{E}$	$\ln \mathcal{E}$	$\ln \mathcal{E}$	Interpretation
Λ CDM	-10.221 ± 0.008	-7.494 ± 0.007	-355.493 ± 0.078	-17.129 ± 0.007	-20.617 ± 0.018	-
ω CDM	-10.371 ± 0.009	-7.899 ± 0.007	-355.618 ± 0.017	-17.519 ± 0.008	-21.061 ± 0.012	Inconclusive
Γ_{a01}	-10.881 ± 0.015	-7.791 ± 0.008	-355.645 ± 0.008	-17.557 ± 0.007	-23.187 ± 0.054	Moderate
Γ_{a02}	-10.268 ± 0.010	-7.900 ± 0.007	-355.641 ± 0.033	-17.280 ± 0.012	-20.864 ± 0.019	Inconclusive
Γ_{a03}	-11.085 ± 0.009	-7.860 ± 0.009	-355.627 ± 0.007	-17.642 ± 0.011	-23.340 ± 0.019	Moderate
Γ_{a04}	-10.890 ± 0.012	-7.907 ± 0.008	-355.690 ± 0.022	-17.663 ± 0.012	-23.259 ± 0.045	Moderate
Γ_{b01}	-10.806 ± 0.013	-7.896 ± 0.008	-355.647 ± 0.023	-17.468 ± 0.015	-23.224 ± 0.046	Moderate
Γ_{b03}	-10.948 ± 0.009	-7.919 ± 0.007	-355.566 ± 0.009	-17.541 ± 0.009	-23.325 ± 0.017	Weak
Γ_{b04}	-10.886 ± 0.013	-7.988 ± 0.014	-355.783 ± 0.018	-17.731 ± 0.019	-23.208 ± 0.074	Moderate
Γ_{c0}	-10.283 ± 0.009	-7.911 ± 0.008	-355.634 ± 0.010	-17.323 ± 0.010	-20.876 ± 0.015	Inconclusive
Γ_{d0}	-10.824 ± 0.011	-7.482 ± 0.014	-355.519 ± 0.033	-17.414 ± 0.035	-22.954 ± 0.106	Weak
Γ_{e0}	-10.290 ± 0.009	-7.895 ± 0.008	-355.596 ± 0.021	-17.407 ± 0.007	-20.812 ± 0.055	Inconclusive
Γ_{a1}	-10.905 ± 0.014	-7.959 ± 0.008	-355.692 ± 0.039	-17.598 ± 0.186	-22.338 ± 0.481	Weak
Γ_{a2}	-10.355 ± 0.011	-7.918 ± 0.013	-355.707 ± 0.021	-17.306 ± 0.014	-20.889 ± 0.044	Inconclusive
Γ_{a3}	-10.988 ± 0.014	-7.851 ± 0.009	-355.694 ± 0.087	-17.784 ± 0.036	-23.232 ± 0.061	Moderate
Γ_{a4}	-10.900 ± 0.015	-7.866 ± 0.011	-355.543 ± 0.208	-17.712 ± 0.015	-23.240 ± 0.082	Moderate
Γ_{b1}	-10.879 ± 0.012	-7.909 ± 0.008	-355.727 ± 0.026	-17.798 ± 0.014	-23.160 ± 0.093	Moderate
Γ_{b2}	-10.439 ± 0.012	-8.039 ± 0.011	-355.468 ± 0.227	-17.544 ± 0.008	-20.907 ± 0.080	Inconclusive
Γ_{b3}	-10.962 ± 0.012	-7.979 ± 0.009	-355.755 ± 0.008	-17.859 ± 0.010	-23.053 ± 0.108	Weak
Γ_{b4}	-10.898 ± 0.013	-7.979 ± 0.009	-355.529 ± 0.318	-17.534 ± 0.047	-23.059 ± 0.093	Weak
Γ_c	-10.387 ± 0.009	-8.033 ± 0.008	-355.688 ± 0.014	-17.332 ± 0.023	-20.793 ± 0.054	Inconclusive
Γ_d	-10.825 ± 0.015	-8.004 ± 0.010	-355.647 ± 0.019	-17.600 ± 0.042	-22.749 ± 0.369	Weak
Γ_e	-10.386 ± 0.009	-7.998 ± 0.100	-355.799 ± 0.009	-17.369 ± 0.009	-20.881 ± 0.051	Inconclusive

Table 7. Bayesian evidence ($\ln \mathcal{E}$) and interpretation for the models considered in this work. Note that $\ln B_i = \ln \mathcal{E}_i - \ln \mathcal{E}_{\Lambda\text{CDM}} < -1$ favors the ΛCDM model.

Dataset	BAO3		BAO3 + CC		BAO3 + CC + CMB	
Model	$\ln \mathcal{E}$	Interpretation	$\ln \mathcal{E}$	Interpretation	$\ln \mathcal{E}$	Interpretation
ΛCDM	-5.218 ± 0.007	-	-11.167 ± 0.008	-	-14.673 ± 0.008	-
ωCDM	-5.559 ± 0.008	Inconclusive	-11.630 ± 0.008	Inconclusive	-14.631 ± 0.206	Inconclusive
Γ_{a01}	-7.037 ± 0.015	Weak	-12.894 ± 0.060	Weak	-17.792 ± 0.031	Moderate
Γ_{a02}	-5.417 ± 0.008	Inconclusive	-11.437 ± 0.008	Inconclusive	-14.770 ± 0.013	Inconclusive
Γ_{a03}	-7.036 ± 0.030	Weak	-13.008 ± 0.027	Weak	-17.824 ± 0.016	Moderate
Γ_{a04}	-6.918 ± 0.018	Weak	-13.083 ± 0.014	Weak	-17.663 ± 0.100	Moderate
Γ_{b01}	-6.910 ± 0.055	Weak	-12.974 ± 0.009	Weak	-17.835 ± 0.018	Moderate
Γ_{b03}	-6.976 ± 0.019	Weak	-12.977 ± 0.008	Weak	-17.788 ± 0.027	Moderate
Γ_{b04}	-6.999 ± 0.036	Weak	-13.354 ± 0.037	Weak	-17.081 ± 0.373	Weak
Γ_{c0}	-5.458 ± 0.010	Inconclusive	-11.439 ± 0.010	Inconclusive	-14.748 ± 0.015	Inconclusive
Γ_{d0}	-7.004 ± 0.016	Weak	-12.929 ± 0.008	Weak	-17.803 ± 0.096	Moderate
Γ_{e0}	-5.441 ± 0.008	Inconclusive	-11.472 ± 0.008	Inconclusive	-14.360 ± 0.264	Inconclusive
Γ_{a1}	-6.979 ± 0.026	Weak	-13.203 ± 0.016	Weak	-17.801 ± 0.024	Moderate
Γ_{a2}	-5.466 ± 0.012	Inconclusive	-11.473 ± 0.015	Inconclusive	-14.759 ± 0.021	Inconclusive
Γ_{a3}	-7.105 ± 0.012	Weak	-13.165 ± 0.101	Weak	-17.644 ± 0.111	Moderate
Γ_{a4}	-6.974 ± 0.026	Weak	-13.143 ± 0.012	Weak	-17.477 ± 0.286	Moderate
Γ_{b1}	-6.974 ± 0.013	Weak	-13.194 ± 0.035	Weak	-17.734 ± 0.044	Moderate
Γ_{b2}	-5.596 ± 0.012	Inconclusive	-11.794 ± 0.008	Inconclusive	-14.621 ± 0.115	Inconclusive
Γ_{b3}	-7.049 ± 0.013	Weak	-13.219 ± 0.017	Weak	-17.605 ± 0.145	Moderate
Γ_{b4}	-6.985 ± 0.021	Weak	-13.269 ± 0.013	Weak	-17.322 ± 0.260	Moderate
Γ_c	-5.515 ± 0.008	Inconclusive	-11.479 ± 0.011	Inconclusive	-14.731 ± 0.013	Inconclusive
Γ_d	-7.026 ± 0.012	Weak	-13.13 ± 0.037	Weak	-17.760 ± 0.037	Moderate
Γ_e	-5.534 ± 0.009	Inconclusive	-11.568 ± 0.008	Inconclusive	-14.691 ± 0.052	Inconclusive

Table 8. Best fit parameters for the joint analysis JLA + BAO2 + CC + CMB. The last three columns show the Bayesian evidence ($\ln \mathcal{E}$), the Bayes factor ($\ln B$) and the interpretation of the strength of the evidence. Note that $\ln B < -1$ favors the Λ CDM model.

Model	h	Ω_{dm}	α	β	γ_x	$\ln \mathcal{E}$	$\ln B$	Interpretation
Λ CDM	0.720 ± 0.008	$0.2127^{+0.0078}_{-0.0088}$	-	-	-	-374.379 ± 0.006	0	-
ω CDM	0.717 ± 0.009	$0.2119^{+0.0078}_{-0.0087}$	-	-	$0.023^{+0.037}_{-0.028}$	-374.120 ± 0.072	0.259 ± 0.072	Inconclusive
Γ_{a01}	0.693 ± 0.020	$0.2166^{+0.0084}_{-0.0094}$	$-0.0077^{+0.0065}_{-0.0045}$	-	-	-376.557 ± 0.063	-2.178 ± 0.063	Weak
Γ_{a02}	0.710 ± 0.011	$0.262^{+0.041}_{-0.034}$	-	$-0.069^{+0.047}_{-0.057}$	-	-373.830 ± 0.160	0.549 ± 0.160	Inconclusive
Γ_{a03}	0.691 ± 0.021	$0.222^{+0.010}_{-0.012}$	$-0.0079^{+0.0064}_{-0.0047}$	$-0.0079^{+0.0064}_{-0.0047}$	-	-375.824 ± 0.290	-1.445 ± 0.290	Weak
Γ_{a04}	0.687 ± 0.020	$0.259^{+0.042}_{-0.034}$	$-0.0065^{+0.0061}_{-0.0041}$	$-0.060^{+0.048}_{-0.058}$	-	-376.222 ± 0.135	-1.843 ± 0.135	Weak
Γ_{b01}	0.692 ± 0.021	$0.2167^{+0.0084}_{-0.0096}$	$0.0079^{+0.0047}_{-0.0068}$	-	-	-376.332 ± 0.259	-1.953 ± 0.259	Weak
Γ_{b03}	0.693 ± 0.021	$0.2165^{+0.0085}_{-0.0098}$	$0.0078^{+0.0046}_{-0.0065}$	$0.0078^{+0.0046}_{-0.0065}$	-	-376.468 ± 0.081	-2.089 ± 0.081	Weak
Γ_{b04}	0.693 ± 0.021	$0.2165^{+0.0086}_{-0.0096}$	$0.0078^{+0.0046}_{-0.0071}$	-0.012 ± 0.097	-	-376.587 ± 0.107	-2.208 ± 0.107	Weak
Γ_{c0}	0.7134 ± 0.0099	0.237 ± 0.024	$-0.075^{+0.057}_{-0.079}$	-	-	-374.004 ± 0.028	0.375 ± 0.029	Inconclusive
Γ_{d0}	0.694 ± 0.021	$0.2142^{+0.0081}_{-0.0091}$	$-0.0076^{+0.0068}_{-0.0047}$	-	-	-376.276 ± 0.224	-1.897 ± 0.224	Weak
Γ_{e0}	0.7173 ± 0.0086	$0.232^{+0.033}_{-0.024}$	$-0.048^{+0.059}_{-0.075}$	-	-	-374.049 ± 0.184	0.330 ± 0.184	Inconclusive
Γ_{a1}	0.690 ± 0.021	$0.2159^{+0.0084}_{-0.0094}$	$-0.0076^{+0.0066}_{-0.0046}$	-	$0.023^{+0.039}_{-0.032}$	-376.373 ± 0.171	-1.994 ± 0.171	Weak
Γ_{a2}	0.710 ± 0.011	$0.255^{+0.045}_{-0.032}$	-	$-0.059^{+0.044}_{-0.062}$	$0.011^{+0.040}_{-0.036}$	-374.116 ± 0.057	0.263 ± 0.057	Inconclusive
Γ_{a3}	0.689 ± 0.021	$0.2214^{+0.0098}_{-0.012}$	$-0.0075^{+0.0063}_{-0.0046}$	$-0.0075^{+0.0063}_{-0.0046}$	$0.020^{+0.038}_{-0.031}$	-376.375 ± 0.150	-1.996 ± 0.150	Weak
Γ_{a4}	0.688 ± 0.020	$0.252^{+0.045}_{-0.038}$	$-0.0064^{+0.0060}_{-0.0042}$	$-0.051^{+0.053}_{-0.061}$	0.011 ± 0.039	-376.557 ± 0.037	-2.178 ± 0.037	Weak
Γ_{b1}	0.691 ± 0.021	0.2159 ± 0.0090	$0.0074^{+0.0046}_{-0.0066}$	-	$0.024^{+0.039}_{-0.033}$	-376.482 ± 0.047	-2.103 ± 0.047	Weak
Γ_{b2}	0.7164 ± 0.0089	0.2124 ± 0.0085	-	0.000 ± 0.095	$0.025^{+0.037}_{-0.029}$	-374.418 ± 0.020	-0.039 ± 0.021	Inconclusive
Γ_{b3}	0.691 ± 0.021	$0.2160^{+0.0084}_{-0.0097}$	$0.0074^{+0.0047}_{-0.0064}$	-	$0.023^{+0.039}_{-0.031}$	-376.492 ± 0.050	-2.113 ± 0.050	Weak
Γ_{b4}	0.690 ± 0.020	0.2159 ± 0.0093	$0.0075^{+0.0045}_{-0.0065}$	-0.007 ± 0.094	$0.024^{+0.038}_{-0.032}$	-376.670 ± 0.040	-2.291 ± 0.040	Weak
Γ_c	0.711 ± 0.010	$0.233^{+0.026}_{-0.023}$	$-0.065^{+0.057}_{-0.082}$	-	$0.019^{+0.038}_{-0.032}$	-374.118 ± 0.022	0.261 ± 0.023	Inconclusive
Γ_d	0.692 ± 0.020	$0.2134^{+0.0080}_{-0.0089}$	$-0.0073^{+0.0065}_{-0.0046}$	-	$0.024^{+0.038}_{-0.031}$	-376.575 ± 0.044	-2.196 ± 0.044	Weak
Γ_e	0.7143 ± 0.0094	$0.227^{+0.034}_{-0.023}$	$-0.036^{+0.056}_{-0.076}$	-	$0.024^{+0.039}_{-0.031}$	-374.271 ± 0.103	0.108 ± 0.103	Inconclusive

Table 9. Best fit parameters for the joint analysis JLA + BAO3 + CC + CMB. The last three columns show the Bayesian evidence ($\ln \mathcal{E}$), the Bayes factor ($\ln B$) and the interpretation of the strength of the evidence. Note that $\ln B < -1$ favors the Λ CDM model.

Model	h	Ω_{dm}	α	β	γ_x	$\ln \mathcal{E}$	$\ln B$	Interpretation
Λ CDM	0.6853 ± 0.0061	0.2537 ± 0.0080	-	-	-	-366.953 ± 0.005	-	
ω CDM	0.6854 ± 0.0081	0.2536 ± 0.0080	-	-	-0.001 ± 0.035	-367.254 ± 0.017	-0.301 ± 0.018	Inconclusive
Γ_{a01}	0.684 ± 0.020	0.2543 ± 0.0088	$-0.0005^{+0.0044}_{-0.0035}$	-	-	-370.216 ± 0.114	-3.263 ± 0.114	Moderate
Γ_{a02}	0.684 ± 0.010	0.259 ± 0.038	-	-0.008 ± 0.052	-	-367.441 ± 0.114	-0.488 ± 0.114	Inconclusive
Γ_{a03}	0.684 ± 0.020	0.255 ± 0.010	$-0.0005^{+0.0044}_{-0.0035}$	$-0.0005^{+0.0044}_{-0.0035}$	-	-370.003 ± 0.150	-3.050 ± 0.150	Moderate
Γ_{a04}	0.683 ± 0.020	0.256 ± 0.039	$-0.0006^{+0.0045}_{-0.0034}$	-0.003 ± 0.053	-	-370.615 ± 0.194	-3.662 ± 0.194	Moderate
Γ_{b01}	0.684 ± 0.020	0.2543 ± 0.0090	$0.0006^{+0.0035}_{-0.0045}$	-	-	-370.091 ± 0.157	-3.138 ± 0.157	Moderate
Γ_{b03}	0.684 ± 0.019	$0.2542^{+0.0083}_{-0.0094}$	$0.0005^{+0.0034}_{-0.0043}$	$0.0005^{+0.0034}_{-0.0043}$	-	-370.286 ± 0.048	-3.333 ± 0.048	Moderate
Γ_{b04}	0.684 ± 0.019	0.2542 ± 0.0087	$0.0005^{+0.0034}_{-0.0043}$	-0.011 ± 0.098	-	-370.193 ± 0.120	-3.240 ± 0.120	Moderate
Γ_{c0}	0.6839 ± 0.0091	0.258 ± 0.025	-0.011 ± 0.068	-	-	-367.110 ± 0.194	-0.157 ± 0.194	Inconclusive
Γ_{d0}	0.684 ± 0.020	0.2542 ± 0.0086	$-0.0007^{+0.0046}_{-0.0035}$	-	-	-370.213 ± 0.058	-3.260 ± 0.058	Moderate
Γ_{e0}	0.6852 ± 0.0075	$0.254^{+0.032}_{-0.027}$	-0.002 ± 0.072	-	-	-367.044 ± 0.078	-0.091 ± 0.078	Inconclusive
Γ_{a1}	0.684 ± 0.020	0.2544 ± 0.0088	$-0.0006^{+0.0044}_{-0.0035}$	-	0.000 ± 0.035	-370.457 ± 0.131	-3.504 ± 0.131	Moderate
Γ_{a2}	0.684 ± 0.010	0.261 ± 0.041	-	-0.011 ± 0.056	-0.004 ± 0.037	-367.683 ± 0.087	-0.730 ± 0.087	Inconclusive
Γ_{a3}	0.684 ± 0.020	$0.2547^{+0.0095}_{-0.011}$	$-0.0005^{+0.0044}_{-0.0034}$	$-0.0005^{+0.0044}_{-0.0034}$	0.001 ± 0.036	-369.561 ± 0.642	-2.608 ± 0.642	Moderate
Γ_{a4}	0.683 ± 0.020	$0.256^{+0.044}_{-0.039}$	$-0.0006^{+0.0045}_{-0.0033}$	-0.004 ± 0.057	-0.002 ± 0.038	-370.905 ± 0.039	-3.952 ± 0.039	Moderate
Γ_{b1}	0.683 ± 0.020	0.2545 ± 0.0088	$0.0006^{+0.0034}_{-0.0045}$	-	0.001 ± 0.035	-370.509 ± 0.055	-3.556 ± 0.055	Moderate
Γ_{b2}	0.6853 ± 0.0080	0.2539 ± 0.0082	-	-0.005 ± 0.093	-0.001 ± 0.034	-367.196 ± 0.030	-0.243 ± 0.030	Inconclusive
Γ_{b3}	0.684 ± 0.020	0.2542 ± 0.0089	$0.0005^{+0.0034}_{-0.0044}$	-	0.000 ± 0.036	-370.416 ± 0.093	-3.463 ± 0.093	Moderate
Γ_{b4}	0.684 ± 0.020	0.2543 ± 0.0092	$0.0007^{+0.0035}_{-0.0045}$	-0.016 ± 0.094	0.000 ± 0.036	-370.560 ± 0.030	-3.607 ± 0.030	Moderate
Γ_c	0.6844 ± 0.0097	0.258 ± 0.026	-0.011 ± 0.072	-	-0.002 ± 0.036	-367.189 ± 0.208	-0.236 ± 0.208	Inconclusive
Γ_d	0.684 ± 0.020	0.2543 ± 0.0084	$-0.0006^{+0.0045}_{-0.0035}$	-	0.000 ± 0.036	-370.328 ± 0.184	-3.375 ± 0.184	Moderate
Γ_e	0.6851 ± 0.0086	$0.254^{+0.031}_{-0.026}$	-0.004 ± 0.069	-	0.000 ± 0.035	-367.306 ± 0.070	-0.353 ± 0.070	Inconclusive

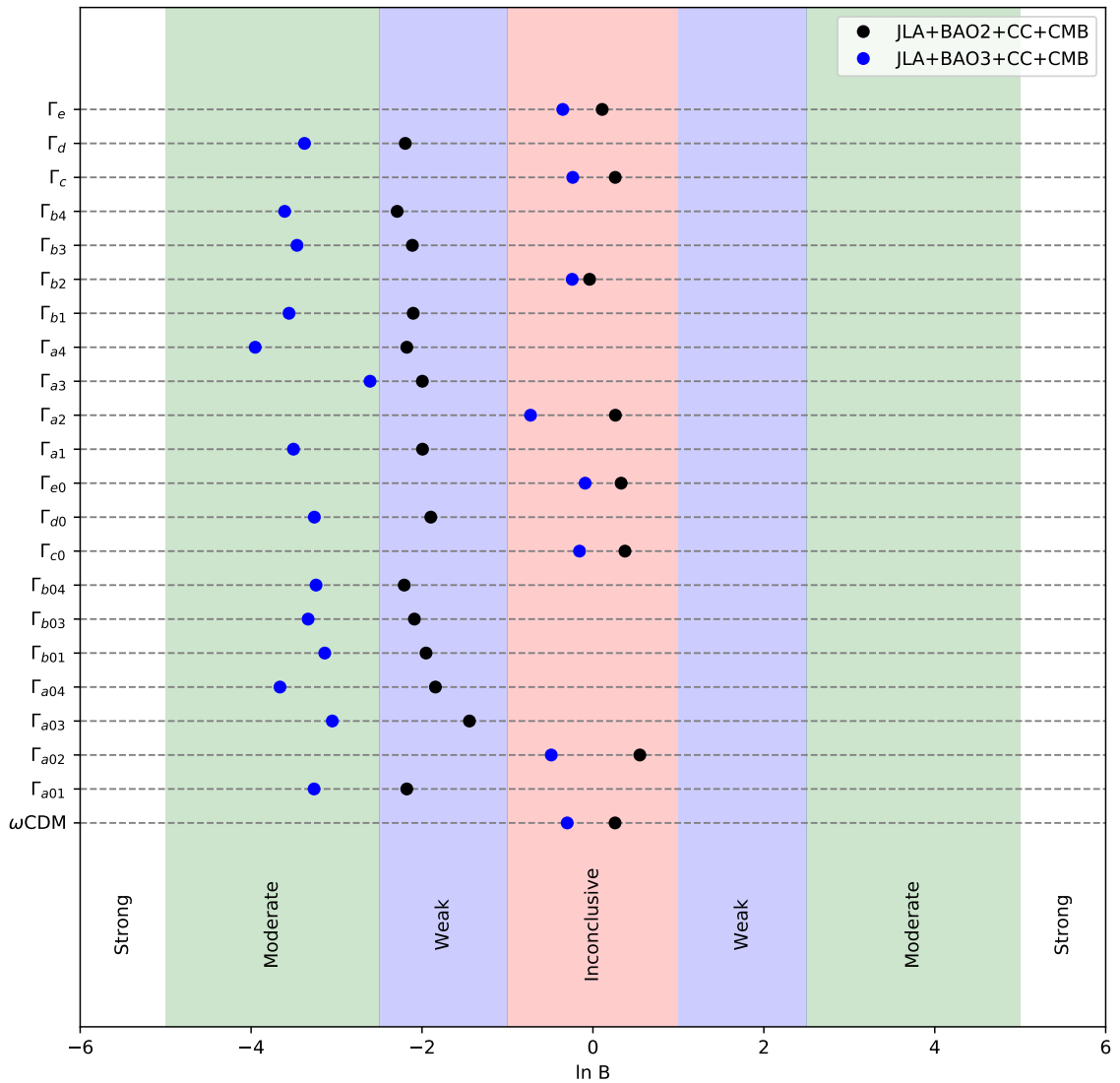


Figure 1. Summary of Bayesian comparison between interacting models and Λ CDM. We show the classification in terms of the Jeffreys' scale, where $\ln B < -1$ favors the Λ CDM scenario.

6 Final Remarks

Relaxing the conventional assumption of a purely gravitational interaction between the dark energy and dark matter components introduces substantial alterations in the predicted evolution of the universe. In this paper, we have performed a Bayesian model selection analysis to compare the observational viability of different classes of interacting models with the standard Λ CDM cosmology. We have found evidence disfavoring (weakly and moderately) about two-thirds of the studied interacting models with respect to Λ CDM when a full joint analysis using JLA + BAO + CC + CMB data is considered. The remaining one-third, however, is able to provide a similar description to the data as the standard cosmology (see Fig. 1). We also notice that some interesting features have emerged in considering independently the full

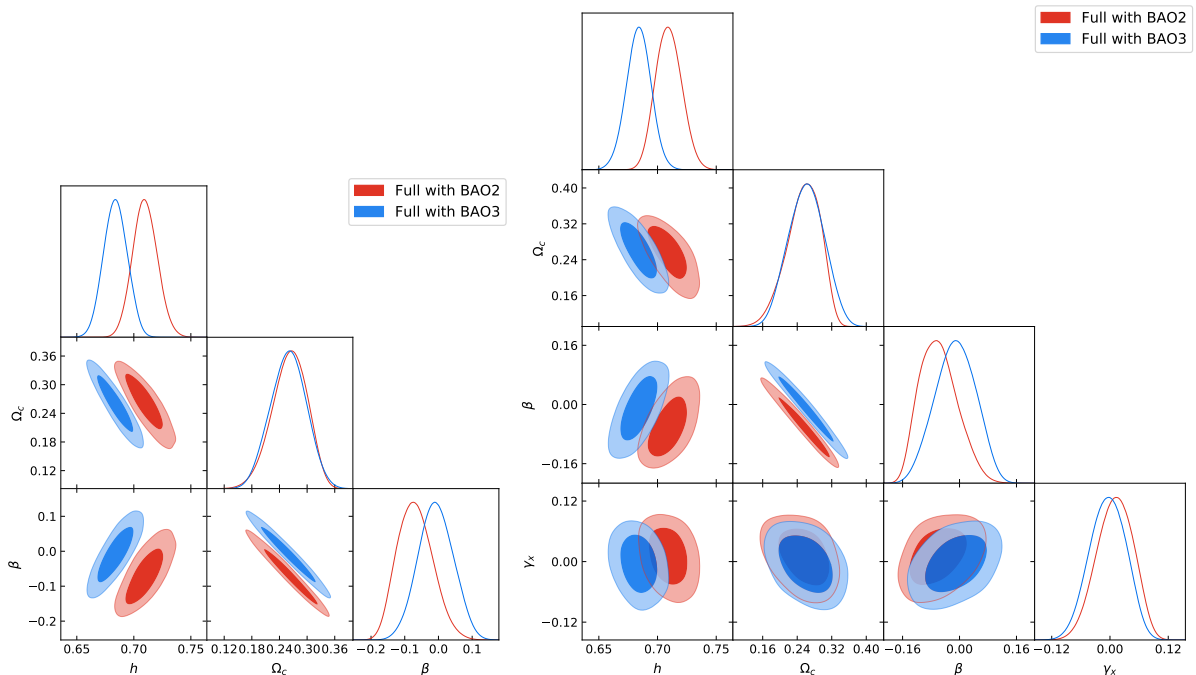


Figure 2. Example of contour plots and PDFs (models Γ_{a02} and Γ_{a2} at left and right, respectively). The figure shows the analysis considering JLA + BAO2 + CC + CMB (red) and JLA + BAO3 + CC + CMB (blue).

analysis using the standard BAO3 measurements and the full analysis using BAO2 measurements, which are more model independent than BAO3 [19]. As can be easily seen in Fig. 1 the evidence disfavoring interacting models are weaker when we use BAO2 instead of BAO3 in the full joint analysis. As mentioned earlier, this result is expected since BAO3 data use Λ CDM as fiducial model, which may introduce a model-dependency in these data. Finally, we emphasize that comparative analysis as the one performed in this paper is important to observationally select viable and non-viable classes of interacting scenarios. As summarized in figure 1, the current observational data are able to select between linear and non-linear interacting terms, showing a slightly preference for the latter type, i.e., among the twenty-one interacting scenarios shown in figure 1 fifteen corresponds to a linear interaction and six to a non-linear interaction. From these, twelve linear scenarios are ruled out with weak or moderate evidence, meanwhile, only two of the non-linear scenarios are ruled out with weak or moderate evidence.

Acknowledgements. AC is partially supported by CONICYT through program Becas Chile de Postdoctorado en el Extranjero grant no. 74170121 and Dirección de Investigación Universidad del Bío-Bío through grant no. GI-172309/C. BS is supported by the DTI-PCI program of the Brazilian Ministry of Science, Technology, and Innovation (MCTI). TF thanks the financial support from CAPES/Brasil. JSA acknowledges support from CNPq (grants no. 310790/2014-0 and 400471/2014-0) and FAPERJ (grant no. 204282). AC would like to thank Javier Gonzalez for his assistance with JLA codes.

References

- [1] D. H. Weinberg, M. J. Mortonson, D. J. Eisenstein, C. Hirata, A. G. Riess, and E. Rozo, *Phys. Rept.* **530**, 87 (2013), [arXiv:1201.2434 \[astro-ph.CO\]](#) .
- [2] S. Weinberg, *Rev. Mod. Phys.* **61**, 1 (1989), [569(1988)].
- [3] S. Weinberg, in *Sources and detection of dark matter and dark energy in the universe. Proceedings, 4th International Symposium, DM 2000, Marina del Rey, USA, February 23-25, 2000* (2000) pp. 18–26, [arXiv:astro-ph/0005265 \[astro-ph\]](#) .
- [4] L. Amendola, *Phys. Rev.* **D62**, 043511 (2000), [arXiv:astro-ph/9908023 \[astro-ph\]](#) .
- [5] W. Zimdahl, D. Pavon, and L. Chimento, *Phys. Lett.* **B521**, 133 (2001), [arXiv:astro-ph/0105479 \[astro-ph\]](#) .
- [6] L. P. Chimento, *Phys. Rev.* **D81**, 043525 (2010), [arXiv:0911.5687 \[astro-ph.CO\]](#) .
- [7] P. C. Ferreira, J. C. Carvalho, and J. S. Alcaniz, *Phys. Rev.* **D87**, 087301 (2013), [arXiv:1212.2492 \[astro-ph.CO\]](#) .
- [8] F. Arevalo, A. Cid, and J. Moya, *Eur. Phys. J.* **C77**, 565 (2017), [arXiv:1610.09330 \[astro-ph.CO\]](#) .
- [9] B. Wang, E. Abdalla, F. Atrio-Barandela, and D. Pavon, *Rept. Prog. Phys.* **79**, 096901 (2016), [arXiv:1603.08299 \[astro-ph.CO\]](#) .
- [10] J. F. Jesus, R. C. Santos, J. S. Alcaniz, and J. A. S. Lima, *Phys. Rev.* **D78**, 063514 (2008), [arXiv:0806.1366 \[astro-ph\]](#) .
- [11] F. E. M. Costa and J. S. Alcaniz, *Phys. Rev.* **D81**, 043506 (2010), [arXiv:0908.4251 \[astro-ph.CO\]](#) .
- [12] F. Arevalo, A. P. R. Bacalhau, and W. Zimdahl, *Class. Quant. Grav.* **29**, 235001 (2012), [arXiv:1112.5095 \[astro-ph.CO\]](#) .
- [13] M. Betoule *et al.* (SDSS), *Astron. Astrophys.* **568**, A22 (2014), [arXiv:1401.4064 \[astro-ph.CO\]](#) .
- [14] F. Beutler, C. Blake, M. Colless, D. H. Jones, L. Staveley-Smith, L. Campbell, Q. Parker, W. Saunders, and F. Watson, *Mon. Not. Roy. Astron. Soc.* **416**, 3017 (2011), [arXiv:1106.3366 \[astro-ph.CO\]](#) .
- [15] A. J. Ross, L. Samushia, C. Howlett, W. J. Percival, A. Burden, and M. Manera, *Mon. Not. Roy. Astron. Soc.* **449**, 835 (2015), [arXiv:1409.3242 \[astro-ph.CO\]](#) .
- [16] A. J. Cuesta *et al.*, *Mon. Not. Roy. Astron. Soc.* **457**, 1770 (2016), [arXiv:1509.06371 \[astro-ph.CO\]](#) .
- [17] M. Ata *et al.*, *Mon. Not. Roy. Astron. Soc.* **473**, 4773 (2018), [arXiv:1705.06373 \[astro-ph.CO\]](#) .
- [18] J. S. Alcaniz, G. C. Carvalho, A. Bernui, J. C. Carvalho, and M. Benetti, *Fundam. Theor. Phys.* **187**, 11 (2017), [arXiv:1611.08458 \[astro-ph.CO\]](#) .
- [19] G. C. Carvalho, A. Bernui, M. Benetti, J. C. Carvalho, and J. S. Alcaniz, *Phys. Rev.* **D93**, 023530 (2016), [arXiv:1507.08972 \[astro-ph.CO\]](#) .
- [20] G. C. Carvalho, A. Bernui, M. Benetti, J. C. Carvalho, and J. S. Alcaniz, (2017), [arXiv:1709.00271 \[astro-ph.CO\]](#) .
- [21] E. de Carvalho, A. Bernui, G. C. Carvalho, and C. P. Novaes, *JCAP* **1804**, 064 (2018), [arXiv:1709.00113 \[astro-ph.CO\]](#) .
- [22] M. Moresco, L. Pozzetti, A. Cimatti, R. Jimenez, C. Maraston, L. Verde, D. Thomas, A. Citro, R. Tojeiro, and D. Wilkinson, *JCAP* **1605**, 014 (2016), [arXiv:1601.01701 \[astro-ph.CO\]](#) .
- [23] P. A. R. Ade *et al.* (Planck), *Astron. Astrophys.* **594**, A14 (2016), [arXiv:1502.01590 \[astro-ph.CO\]](#) .

- [24] U. Debnath, *Astrophys. Space Sci.* **312**, 295 (2007), [arXiv:0710.1708 \[gr-qc\]](#) .
- [25] H. M. Sadjadi and M. Alimohammadi, *Phys. Rev.* **D74**, 103007 (2006), [arXiv:gr-qc/0610080 \[gr-qc\]](#) .
- [26] N. Dalal, K. Abazajian, E. E. Jenkins, and A. V. Manohar, *Phys. Rev. Lett.* **87**, 141302 (2001), [arXiv:astro-ph/0105317 \[astro-ph\]](#) .
- [27] Y.-H. Li and X. Zhang, *Phys. Rev.* **D89**, 083009 (2014), [arXiv:1312.6328 \[astro-ph.CO\]](#) .
- [28] D. J. Eisenstein *et al.* (SDSS), *Astrophys. J.* **633**, 560 (2005), [arXiv:astro-ph/0501171 \[astro-ph\]](#) .
- [29] D. J. Eisenstein and W. Hu, *Astrophys. J.* **496**, 605 (1998), [arXiv:astro-ph/9709112 \[astro-ph\]](#) .
- [30] P. A. R. Ade *et al.* (Planck), *Astron. Astrophys.* **594**, A13 (2016), [arXiv:1502.01589 \[astro-ph.CO\]](#) .
- [31] F. Beutler, C. Blake, J. Koda, F. Marin, H.-J. Seo, A. J. Cuesta, and D. P. Schneider, *Mon. Not. Roy. Astron. Soc.* **455**, 3230 (2016), [arXiv:1506.03900 \[astro-ph.CO\]](#) .
- [32] J. Sollerman *et al.*, *Astrophys. J.* **703**, 1374 (2009), [arXiv:0908.4276 \[astro-ph.CO\]](#) .
- [33] R. J. Cooke, M. Pettini, K. M. Nollett, and R. Jorgenson, *Astrophys. J.* **830**, 148 (2016), [arXiv:1607.03900 \[astro-ph.CO\]](#) .
- [34] R. Jimenez and A. Loeb, *Astrophys. J.* **573**, 37 (2002), [arXiv:astro-ph/0106145 \[astro-ph\]](#) .
- [35] G. Bruzual and S. Charlot, *Mon. Not. Roy. Astron. Soc.* **344**, 1000 (2003), [arXiv:astro-ph/0309134 \[astro-ph\]](#) .
- [36] J. Simon, L. Verde, and R. Jimenez, *Phys. Rev.* **D71**, 123001 (2005), [arXiv:astro-ph/0412269 \[astro-ph\]](#) .
- [37] L. Verde, P. Protopapas, and R. Jimenez, *Phys. Dark Univ.* **5-6**, 307 (2014), [arXiv:1403.2181 \[astro-ph.CO\]](#) .
- [38] M. Moresco *et al.*, *JCAP* **1208**, 006 (2012), [arXiv:1201.3609 \[astro-ph.CO\]](#) .
- [39] C. Zhang, H. Zhang, S. Yuan, T.-J. Zhang, and Y.-C. Sun, *Res. Astron. Astrophys.* **14**, 1221 (2014), [arXiv:1207.4541 \[astro-ph.CO\]](#) .
- [40] D. Stern, R. Jimenez, L. Verde, M. Kamionkowski, and S. A. Stanford, *JCAP* **1002**, 008 (2010), [arXiv:0907.3149 \[astro-ph.CO\]](#) .
- [41] M. Sako *et al.* (SDSS), (2014), [arXiv:1401.3317 \[astro-ph.CO\]](#) .
- [42] A. Conley *et al.* (SNLS), *Astrophys. J. Suppl.* **192**, 1 (2011), [arXiv:1104.1443 \[astro-ph.CO\]](#) .
- [43] J. Guy *et al.* (SNLS), *Astron. Astrophys.* **523**, A7 (2010), [arXiv:1010.4743 \[astro-ph.CO\]](#) .
- [44] A. G. Riess *et al.*, *Astrophys. J.* **659**, 98 (2007), [arXiv:astro-ph/0611572 \[astro-ph\]](#) .
- [45] B. Santos, N. C. Devi, and J. S. Alcaniz, *Phys. Rev.* **D95**, 123514 (2017), [arXiv:1603.06563 \[astro-ph.CO\]](#) .
- [46] A. Heavens, Y. Fantaye, E. Sellentin, H. Eggers, Z. Hosenie, S. Kroon, and A. Mootooyaloo, *Phys. Rev. Lett.* **119**, 101301 (2017), [arXiv:1704.03467 \[astro-ph.CO\]](#) .
- [47] S. Santos da Costa, M. Benetti, and J. Alcaniz, *JCAP* **1803**, 004 (2018), [arXiv:1710.01613 \[astro-ph.CO\]](#) .
- [48] U. Andrade, C. A. P. Bengaly, J. S. Alcaniz, and B. Santos, *Phys. Rev.* **D97**, 083518 (2018), [arXiv:1711.10536 \[astro-ph.CO\]](#) .
- [49] T. Ferreira, C. Pigozzo, S. Carneiro, and J. S. Alcaniz, (2017), [arXiv:1712.05428 \[astro-ph.CO\]](#) .
- [50] A. R. Liddle, *Mon. Not. Roy. Astron. Soc.* **377**, L74 (2007), [arXiv:astro-ph/0701113 \[astro-ph\]](#) .

- [51] A. Lewis and S. Bridle, *Phys. Rev. D* **66**, 103511 (2002), [arXiv:astro-ph/0205436 \[astro-ph\]](#) .
- [52] P. Mukherjee, D. Parkinson, and A. R. Liddle, *Astrophys. J.* **638**, L51 (2006), [arXiv:astro-ph/0508461 \[astro-ph\]](#) .
- [53] J. Skilling, *AIP Conf. Proc.* **735**, 395 (2004).
- [54] F. Feroz and M. P. Hobson, *Mon. Not. Roy. Astron. Soc.* **384**, 449 (2008), [arXiv:0704.3704 \[astro-ph\]](#) .
- [55] F. Feroz, M. P. Hobson, and M. Bridges, *Mon. Not. Roy. Astron. Soc.* **398**, 1601 (2009), [arXiv:0809.3437 \[astro-ph\]](#) .
- [56] F. Feroz, M. P. Hobson, E. Cameron, and A. N. Pettitt, ArXiv e-prints (2013), [arXiv:1306.2144 \[astro-ph.IM\]](#) .
- [57] H. Jeffreys, *Theory of Probability*, 3rd ed. (Oxford Univ. Press, Oxford, England, 1961).
- [58] R. Trotta, *Contemp. Phys.* **49**, 71 (2008), [arXiv:0803.4089 \[astro-ph\]](#) .
- [59] A. G. Riess *et al.*, *Astrophys. J.* **826**, 56 (2016), [arXiv:1604.01424 \[astro-ph.CO\]](#) .
- [60] D. Pavon and B. Wang, *Gen. Rel. Grav.* **41**, 1 (2009), [arXiv:0712.0565 \[gr-qc\]](#) .
- [61] E. Komatsu *et al.* (WMAP), *Astrophys. J. Suppl.* **192**, 18 (2011), [arXiv:1001.4538 \[astro-ph.CO\]](#) .
- [62] G. Mangano, G. Miele, S. Pastor, T. Pinto, O. Pisanti, and P. D. Serpico, *Nucl. Phys.* **B729**, 221 (2005), [arXiv:hep-ph/0506164 \[hep-ph\]](#) .
- [63] M. Benetti, L. L. Graef, and J. S. Alcaniz, (2017), [arXiv:1712.00677 \[astro-ph.CO\]](#) .
- [64] W. J. Percival *et al.* (SDSS), *Mon. Not. Roy. Astron. Soc.* **401**, 2148 (2010), [arXiv:0907.1660 \[astro-ph.CO\]](#) .
- [65] K. T. Mehta, A. J. Cuesta, X. Xu, D. J. Eisenstein, and N. Padmanabhan, *Mon. Not. Roy. Astron. Soc.* **427**, 2168 (2012), [arXiv:1202.0092 \[astro-ph.CO\]](#) .
- [66] L. Anderson *et al.* (BOSS), *Mon. Not. Roy. Astron. Soc.* **441**, 24 (2014), [arXiv:1312.4877 \[astro-ph.CO\]](#) .
- [67] C. Blake *et al.*, *Mon. Not. Roy. Astron. Soc.* **418**, 1707 (2011), [arXiv:1108.2635 \[astro-ph.CO\]](#) .
- [68] E. A. Kazin *et al.*, *Mon. Not. Roy. Astron. Soc.* **441**, 3524 (2014), [arXiv:1401.0358 \[astro-ph.CO\]](#) .
- [69] D. J. Eisenstein, H.-j. Seo, E. Sirko, and D. Spergel, *Astrophys. J.* **664**, 675 (2007), [arXiv:astro-ph/0604362 \[astro-ph\]](#) .
- [70] N. Padmanabhan, X. Xu, D. J. Eisenstein, R. Scalzo, A. J. Cuesta, K. T. Mehta, and E. Kazin, *Mon. Not. Roy. Astron. Soc.* **427**, 2132 (2012), [arXiv:1202.0090 \[astro-ph.CO\]](#) .
- [71] S. Anselmi, G. D. Starkman, P.-S. Corasaniti, R. K. Sheth, and I. Zehavi, (2017), [arXiv:1703.01275 \[astro-ph.CO\]](#) .
- [72] T. Delubac *et al.* (BOSS), *Astron. Astrophys.* **574**, A59 (2015), [arXiv:1404.1801 \[astro-ph.CO\]](#) .

A BAO data

In using BAO data shown in table 10 we have to consider some issues pointed out in the literature. For instance, in order to obtain the BAO signal from galaxy catalogues through the 2-point correlation function, it is necessary to assume a fiducial model in order to transform redshift into comoving distances [64]. On the other hand, the fiducial model considered in the literature (usually the Λ CDM model) assumes different values for the cosmological parameters

and consequently the derived r_d^{fid} value results to be different in each case. Besides, to compute r_d^{fid} authors use the Eisenstein's or CAMB formulas which could bring discrepancies in using these data combined to constrain cosmological models [65].

In table 10 we show the current available BAO measurements, here we have not included the data reported in references [66] or [67] given that these measurements have been re-analyzed in references [16] and [68], respectively. In these last references the authors apply the reconstruction of the baryonic acoustic feature technique [69, 70] to the former measurements. This reconstruction method leads to a more precise determination of the BAO signal, but the cost is to introduce model dependencies into the BAO data (see the discussion in reference [71]).

Finally, it is worth to point it out that references [72] and [17] are using quasars samples to detect the BAO signal at high redshifts whereas all the other measurements are performed from galaxy samples.

Table 10. The most up to date BAO measurements available in the literature.

Survey	z_{eff}	Reported Parameter	Redshift Sample	r_d^{fid} [Mpc]	Ref. / Year
SDSS DR7	0.200	$d_z^{-1} = 0.1905 \pm 0.0061$	$0.00 < z < 0.50$	154.70	[64] 2010
SDSS DR7	0.350	$d_z^{-1} = 0.1097 \pm 0.0036$	$0.00 < z < 0.50$	154.70	[64] 2010
SDSS DR7	0.275	$d_z^{-1} = 0.1390 \pm 0.0037$	$0.00 < z < 0.50$	154.70	[64] 2010
6dFGS	0.106	$d_z^{-1} = 0.3360 \pm 0.0150$	$0.00 < z < 0.24$	–	[14] 2011
SDSS DR7	0.350	$d_z = (8.88 \pm 0.17)r_d$	$0.15 < z < 0.50$	154.25	[70] 2012
WiggleZ	0.440	$d_z = (1716 \pm 83)/r_d^{\text{fid}}$	$0.20 < z < 1.00$	148.60	[68] 2014
WiggleZ	0.600	$d_z = (2221 \pm 101)/r_d^{\text{fid}}$	$0.20 < z < 1.00$	148.60	[68] 2014
WiggleZ	0.730	$d_z = (2516 \pm 86)/r_d^{\text{fid}}$	$0.20 < z < 1.00$	148.60	[68] 2014
BOSS Ly α F	2.340	$D_A = (11.28 \pm 0.65)r_d$	$2.10 \leq z \leq 3.50$	149.70	[72] 2015
BOSS Ly α F	2.340	$D_H = (9.18 \pm 0.28)r_d$	$2.10 \leq z \leq 3.50$	149.70	[72] 2015
SDSS MGS	0.150	$d_z = (664 \pm 25)/r_d^{\text{fid}}$	$0.00 < z < 0.20$	148.69	[15] 2015
BOSS LOWZ	0.320	$d_z = (1264 \pm 22)/r_d^{\text{fid}}$	$0.15 < z < 0.43$	147.10	[16] 2016
BOSS CMASS	0.570	$d_z = (2028 \pm 21)/r_d^{\text{fid}}$	$0.43 < z < 0.70$	147.10	[16] 2016
eBOSS	1.520	$d_z = (3855 \pm 170)/r_d^{\text{fid}}$	$0.80 < z < 2.20$	147.78	[17] 2017